

# Enhanced Photoresponsive Ultrathin Graphitic-Phase $C_3N_4$ Nanosheets for Bioimaging

Xiaodong Zhang, Xiao Xie, Hui Wang, Jiajia Zhang, Bikai Pan, and Yi Xie\*

Hefei National Laboratory for Physical Science at Microscale, University of Science and Technology of China, Hefei, Anhui, 230026, P. R. China

**S** Supporting Information

**ABSTRACT:** Two-dimensional nanosheets have attracted tremendous attention because of their promising practical application and theoretical values. The atomic-thick nanosheets are able to not only enhance the intrinsic properties of their bulk counterparts but also give birth to new promising properties. Herein, we highlight an available pathway to prepare the ultrathin graphitic-phase  $C_3N_4$  (g- $C_3N_4$ ) nanosheets by a “green” liquid exfoliation route from bulk g- $C_3N_4$  in water for the first time. The as-obtained ultrathin g- $C_3N_4$  nanosheet solution is very stable in both the acidic and alkaline environment and shows pH-dependent photoluminescence (PL). Compared to the bulk g- $C_3N_4$ , ultrathin g- $C_3N_4$  nanosheets show enhanced intrinsic photoabsorption and photoresponse, which induce their extremely high PL quantum yield up to 19.6%. Thus, benefiting from the inherent blue light PL with high quantum yields and high stability, good biocompatibility, and nontoxicity, the water-soluble ultrathin g- $C_3N_4$  nanosheet is a brand-new but promising candidate for bioimaging application.

Ultrathin two-dimensional (2D) nanosheets have attracted extensive attention from scientists for their exceptional electronic, optical, and biocompatible properties with respect to the bulk materials and are suitable for practical applications in effectively connecting microscopic and macroscopic processes.<sup>1</sup> Since the discovery of graphene, great efforts have been undertaken to synthesize atomic-thick nanosheets of both the intrinsically layered structural and nonlayered structural materials and explore their abundant properties.<sup>2</sup> For example, graphene and graphene oxide (GO) nanosheets have been applied in transparent conducting electrodes, supercapacitors, bioimaging and biomedical applications, and so on.<sup>3</sup> In recent decades, the traditional luminescent semiconductors due to their high photoluminescence (PL) quantum yields and size-dependent emission have long been applied in bioimaging and biomedical areas.<sup>4</sup> However, the heavy-metal containing materials with perceptive toxicity definitely hampered further in vivo and in vitro applications.<sup>5</sup> For the absence of any metal elements, graphene based materials possessing relatively high biocompatibility are considered as promising alternatives to traditional luminescent semiconductors for bioimaging and biomedical applications. However, the graphene based materials still exhibit low photoresponse in aqueous solution and are often functionalized by biocompatible molecules to improve their

biocompatibility;<sup>3c,6</sup> in that case, exploring new metal-free materials with high photoresponsivity and biocompatibility is urgently needed.

Recently reported metal-free graphitic-phase  $C_3N_4$  (g- $C_3N_4$ ) with high PL intensity provided inspiration as a potential candidate for bioimaging and biomedical applications.<sup>7</sup> The g- $C_3N_4$  possesses a graphite-like structure, with weak van der Waals force between C–N layers, and a layer distance of about 3.3 nm.<sup>8,9a</sup> Since first reported, g- $C_3N_4$  has been applied in many areas, but most are limited in regards to photocurrent, photoreactivity, and electrocatalysis based on its proper band gap of about 2.7 eV.<sup>9</sup> Though possessing high PL intensity, the bulk g- $C_3N_4$  is not suitable for bioimaging and biomedical applications, due to its low photoresponsivity and the macroscopic size.

Atomically thick 2D nanosheets can promote the photoresponse with respect to bulk materials, which has been demonstrated in many cases.<sup>10,11</sup> Bearing this fact in mind, we propose here that reducing the macroscopic 3D g- $C_3N_4$  into a microscopic 2D structure, as in the case of the graphite to graphene based materials, should result in enhanced photoresponsivity, which may be suitable for bioimaging and biomedical applications in the case of proper size distribution. Therefore, we carried out first-principle density-functional (DFT) calculations to study the electronic structure of the bulk and single-layered nanosheet of g- $C_3N_4$ , respectively. As shown in Figure 1a, the calculated density of states (DOS) of single-layered g- $C_3N_4$  nanosheets shows an obvious increase of DOS at the conduction band edge with respect to the bulk counterpart, indicating the atomically thick g- $C_3N_4$  nanosheets possess more charge carriers. In that case, one can anticipate that the 2D ultrathin g- $C_3N_4$  nanosheets will show improved photoresponsivity.<sup>10,12</sup> Figure 1b,d shows the wave functions of the valence bands of bulk and single-layered g- $C_3N_4$ , respectively, which are mainly derived from the p orbital of nitrogen. However, the corresponding wave functions of the conduction bands (Figure 1c,e) are derived from the combination of the p orbitals of carbon and nitrogen. Compared with bulk g- $C_3N_4$ , the wave functions of the valence band and corresponding conduction band of single-layered g- $C_3N_4$  show enhanced p orbital hybridization of carbon and nitrogen, especially of the conduction band. So, it can be deduced from just the enhanced orbital hybridization that the DOS of single-

Received: August 28, 2012

Published: December 17, 2012



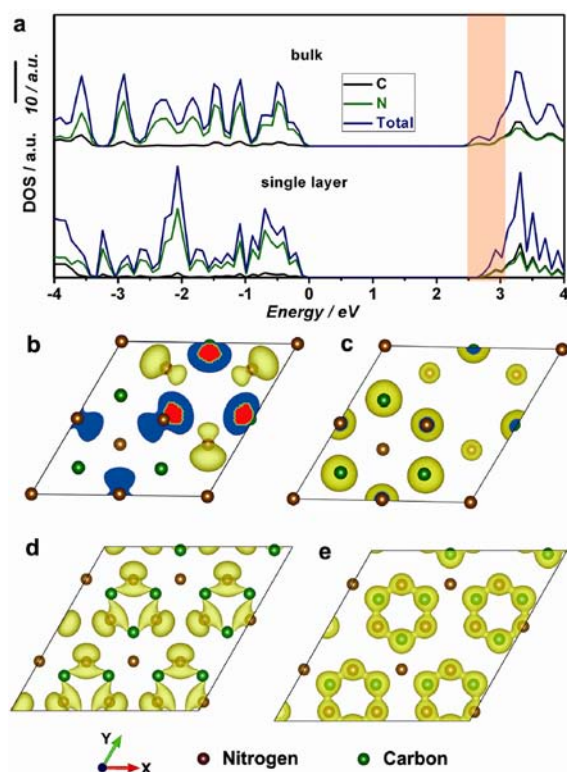


**Figure 1.** (a) Calculated density of states (DOS) of the single-layered  $g\text{-C}_3\text{N}_4$  nanosheet and bulk  $g\text{-C}_3\text{N}_4$ . The shadow part clearly indicates the increase of DOS at the conduction band edge of the  $g\text{-C}_3\text{N}_4$  nanosheet. (b and c) The Kohn–Sham orbitals for the valence band and corresponding conduction band of bulk  $g\text{-C}_3\text{N}_4$ , respectively. (d and e) The Kohn–Sham orbitals for the valence band and corresponding conduction band of single-layered  $g\text{-C}_3\text{N}_4$ , respectively.

layered  $g\text{-C}_3\text{N}_4$  shows an obvious increase in the conduction band edge with respect to the bulk counterpart.

The recently developed liquid exfoliation process is considered to be an effective pathway to prepare the ultrathin 2D nanosheets of intrinsically layered structural materials with high quality.<sup>13</sup> Accordingly, the layered structure  $g\text{-C}_3\text{N}_4$  is expected to be easily exfoliated into ultrathin nanosheets. The exfoliation efficiency of the liquid-exfoliation process can be estimated by the enthalpy of mixing ( $\Delta H_{\text{mix}}$ ), which would be minimized when the surface energies of the solvent and bulk  $g\text{-C}_3\text{N}_4$  match each other. The relationship between the surface energy and mixing enthalpy can be described in the following equation:<sup>13b</sup>

$$\frac{\Delta H_{\text{mix}}}{V_{\text{mix}}} = \frac{2}{T_{\text{bulk}}} (\delta_{\text{G}} - \delta_{\text{sol}})^2 \phi$$

where  $\delta$  is the square root of the component surface energy,  $T_{\text{bulk}}$  is the average thickness of the bulk, and  $\phi$  is the volume fraction of  $g\text{-C}_3\text{N}_4$ . To handle this issue, we theoretically calculated the surface energy of  $g\text{-C}_3\text{N}_4$  by the Grimme parametrized DFT-D2 method.<sup>14</sup> The calculated surface energy is about 115 mJ/m<sup>2</sup>, which matches well with the surface energy of H<sub>2</sub>O (~102 mJ/m<sup>2</sup>), indicating water with the remarkable dispersing efficiency of  $g\text{-C}_3\text{N}_4$  nanosheets. Also, structural analysis showed that, different from graphite, there are dangling hydrogens in the C–N layers of  $g\text{-C}_3\text{N}_4$ , which are usually derived from thermal polycondensation of cyanamide or related Dicyandiamide, melamine molecules during the preparation process.<sup>15</sup> In that case, the polarity solvents will be effective for swelling and then

exfoliating the bulk  $g\text{-C}_3\text{N}_4$  into ultrathin nanosheets. Herein, we highlight an available pathway for the large-scale synthesis of ultrathin  $g\text{-C}_3\text{N}_4$  nanosheets by a “green” liquid exfoliation route from bulk  $g\text{-C}_3\text{N}_4$  in water. We carried out the exfoliation experiments by several solvents with different polarity, in which only H<sub>2</sub>O can effectively exfoliate the  $g\text{-C}_3\text{N}_4$  into ultrathin nanosheets, benefiting from the highest polarity among the used solvents and its matching of surface energy with bulk  $g\text{-C}_3\text{N}_4$  (Table S1, Figure S6). As illustrated in Figure 2a,b, the yellow  $g\text{-C}_3\text{N}_4$

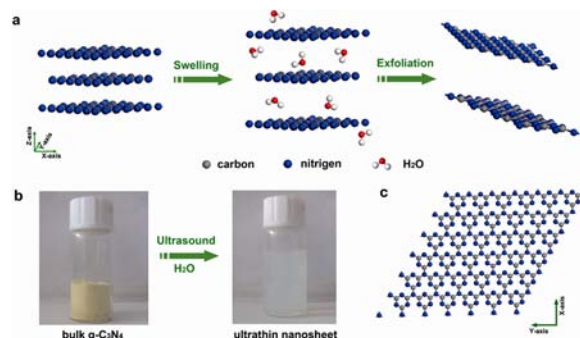


**Figure 2.** (a) Schematic illustration of liquid-exfoliation process from bulk  $g\text{-C}_3\text{N}_4$  to ultrathin nanosheets. (b) Photograph of bulk  $g\text{-C}_3\text{N}_4$  and suspension of ultrathin  $g\text{-C}_3\text{N}_4$  nanosheets. (c) A theoretically perfect crystal structure of the  $g\text{-C}_3\text{N}_4$  projected along the  $z$ -axis.

$\text{C}_3\text{N}_4$  bulk materials can be swelled and then exfoliated into the nearly transparent ultrathin nanosheets by water with the concentration estimated to be about 0.15 mg/mL. The dispersed ultrathin  $g\text{-C}_3\text{N}_4$  nanosheets were negatively charged, with a zeta potential of about  $-30.3$  mV (Figure S5). Benefiting from the highly negative surface charge, the solution of ultrathin  $g\text{-C}_3\text{N}_4$  nanosheets is very stable, without aggregating upon standing for more than several months. Furthermore, the aqueous solution of ultrathin  $g\text{-C}_3\text{N}_4$  nanosheets can be stable under an acidic or alkaline environment with pH values ranging from 3 to 11 (Figure S7). For the absence of any high temperature treatment or oxidation process, the exfoliated nanosheets will retain the same crystal structure and chemical stoichiometric ratio of bulk materials, which will reflect the intrinsic properties of  $g\text{-C}_3\text{N}_4$ .

Figure 3a is the transmission electron microscopy (TEM) image of the exfoliated product, showing free-standing nanosheets with a diameter of ~120 nm. Also, the nearly transparent feature of the nanosheets indicates its ultrathin thickness. The well-defined Tyndall effect of the  $g\text{-C}_3\text{N}_4$  nanosheet solution as displayed in the inset of Figure 3a indicates the presence of highly monodisperse ultrathin nanosheets in water. The X-ray diffraction (XRD) pattern of the  $g\text{-C}_3\text{N}_4$  nanosheet films by vacuum filtration shows only one peak of (002) of the  $g\text{-C}_3\text{N}_4$  crystal (Figure S10), indicating that the nanosheet films assembled by the exfoliated nanosheets displaying the  $xy$ -plane are in a good  $z$ -orientation compared with the bulk  $g\text{-C}_3\text{N}_4$  powders. The size distribution of as-prepared  $g\text{-C}_3\text{N}_4$  nanosheets was evaluated from the tapping mode atomic force microscopy (AFM) image (Figure S9) by measuring the diameter of ~100 nanosheets. As can be seen from Figure 3b, the diameter of the nanosheets ranges from 70 to 160 nm; as they are mainly in the 100 nm region, the likelihood of in vivo or in vitro bioimaging application is increased. As shown in Figure 3c,d, the randomly measured nanosheets are nearly the same thickness (~2.5 nm), indicating the exfoliated nanosheets are comprised of only about seven C–N layers. In addition, the ultrathin  $g\text{-C}_3\text{N}_4$  nanosheets

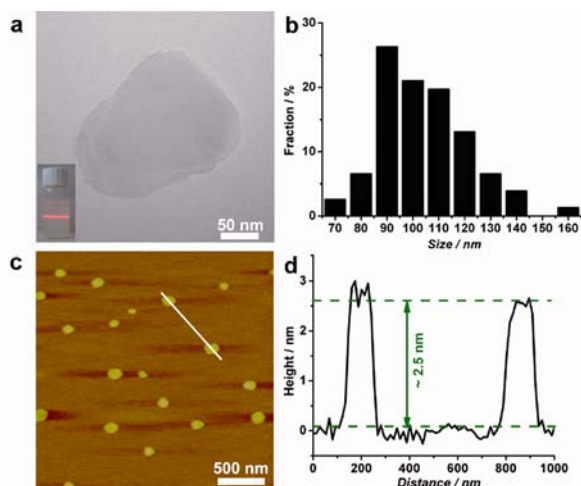


**Figure 3.** (a) TEM image of the ultrathin  $g\text{-C}_3\text{N}_4$  nanosheet; inset of (a) is the Tyndall effect of the ultrathin  $g\text{-C}_3\text{N}_4$  nanosheet dispersed in water. (b) Size distribution of as-prepared  $g\text{-C}_3\text{N}_4$  nanosheets evaluated from the AFM image of Figure S9. (c) AFM image of the synthetic  $g\text{-C}_3\text{N}_4$  nanosheets. (d) The corresponding height image of two random nanosheets.

can be facily assembled into large-area films with tunable thickness, structural integrity, and flexibility for further practical applications (Figure S11).

The electronic structure of as-prepared ultrathin  $g\text{-C}_3\text{N}_4$  nanosheets was studied by the combined analysis of their optical absorption and PL spectra. As shown in Figure 4a, the intrinsic

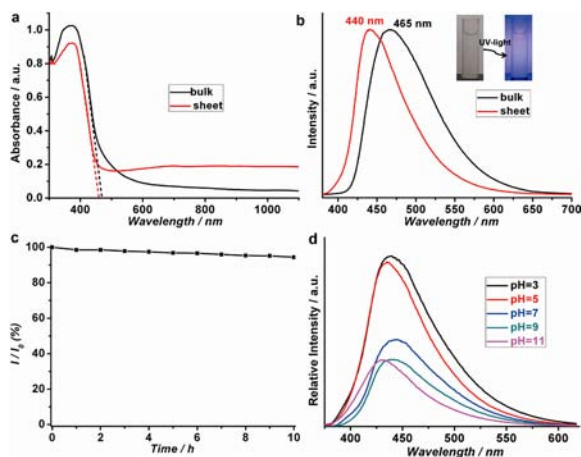


**Figure 4.** (a) UV-visible absorption spectra. (b) Normalized photoluminescence spectra of bulk  $g\text{-C}_3\text{N}_4$  and ultrathin  $g\text{-C}_3\text{N}_4$  nanosheets; inset of (b) is the color change of ultrathin  $g\text{-C}_3\text{N}_4$  nanosheets solution before and under UV light illumination. (c) Dependence of PL intensity on UV-light illumination time for ultrathin  $g\text{-C}_3\text{N}_4$  nanosheet solution. (d) The pH-dependent PL behavior of ultrathin  $g\text{-C}_3\text{N}_4$  nanosheet aqueous solution.

absorption edge of ultrathin  $g\text{-C}_3\text{N}_4$  nanosheets shows a slight blue shift in comparison with the bulk  $g\text{-C}_3\text{N}_4$ , and the band gap of bulk  $g\text{-C}_3\text{N}_4$  of  $\sim 2.64$  eV increased to 2.70 eV for ultrathin  $g\text{-C}_3\text{N}_4$  nanosheets. At the same time, the absorption spectra of ultrathin  $g\text{-C}_3\text{N}_4$  nanosheets extend to the whole visible light region and even the infrared region, enhancing the absorbance of light.<sup>16</sup> In that case, the ultrathin  $g\text{-C}_3\text{N}_4$  nanosheets will show enhanced photoresponsivity with respect to the bulk  $g\text{-C}_3\text{N}_4$ , in accordance with the above theoretical prediction results. As

illustrated in Figure S12, the ultrathin  $g\text{-C}_3\text{N}_4$  nanosheets show enhanced intrinsic photocurrent and photocatalytic activity compared with the bulk sample, because of the improved photoabsorption and photoresponsivity. Furthermore, the photoluminescence (PL) spectra of ultrathin  $g\text{-C}_3\text{N}_4$  nanosheets show a blue shift of  $\sim 20$  nm compared with the bulk  $g\text{-C}_3\text{N}_4$  (Figure 4b). The blue shift of both the band gap and PL spectra can be ascribed to the quantum confinement effect with the conduction and valence band shifting in opposite directions. As shown in the inset of Figure 4b, under UV-light the ultrathin  $g\text{-C}_3\text{N}_4$  nanosheets emit blue PL, and the PL intensity of ultrathin  $g\text{-C}_3\text{N}_4$  nanosheets is very stable with no obvious photobleaching loss after irradiation with a Hg-lamp for even 10 h (Figure 4c). Interestingly, the ultrathin  $g\text{-C}_3\text{N}_4$  nanosheets show pH-dependent PL behavior, in which the PL intensity decreases with increasing pH. As illustrated in Figure 4d, the  $g\text{-C}_3\text{N}_4$  nanosheet solution shows higher PL intensity under acidic conditions but drops intensively when under alkaline conditions, with both showing a slight blue shift with respect to the PL spectra under pH = 7. This pH-dependent PL behavior of ultrathin  $g\text{-C}_3\text{N}_4$  nanosheets can be partially ascribed to the presence of free zigzag sites just as the previously reported graphene quantum dots (GQD) for a similar structure between  $g\text{-C}_3\text{N}_4$  and graphene.<sup>17</sup> It is worth noting that, benefiting from the enhanced photoresponsivity, the ultrathin  $g\text{-C}_3\text{N}_4$  nanosheets show an extremely high PL quantum yield of about 19.6%, much higher than the value for bulk  $g\text{-C}_3\text{N}_4$  (4.8%) and the well-known water-soluble GQD.<sup>6</sup> The high PL quantum yield and PL stability of the water-soluble ultrathin  $g\text{-C}_3\text{N}_4$  nanosheets endow them as a promising candidate for bioimaging application.

The biocompatibility of the ultrathin  $g\text{-C}_3\text{N}_4$  nanosheets was evaluated by the viability of HeLa cells after incubation with the nanosheets for 48 h by an MTT (3-(4,5-dimethylthiazol-2-yl)-3,5-diphenyltetrazolium bromide) assay. As can be seen from Figure 5a, no apparent loss of cell viability was observed even with the concentration of incubated  $g\text{-C}_3\text{N}_4$  nanosheets as high as 600  $\mu\text{g/mL}$ , indicating the excellent biocompatibility and

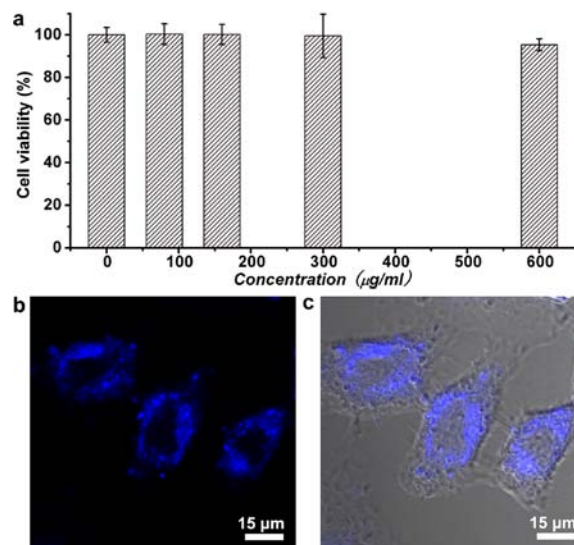


**Figure 5.** (a) Viability of HeLa cells after 48 h of incubation with different concentrations of ultrathin  $g\text{-C}_3\text{N}_4$  nanosheets. (b) Confocal fluorescence image and (c) overlay image of bright field and confocal fluorescence image of the HeLa cells incubated with ultrathin  $g\text{-C}_3\text{N}_4$  nanosheets for about 1 h.

nontoxicity of the ultrathin g-C<sub>3</sub>N<sub>4</sub> nanosheets. It is worth noting that the concentration of incubated ultrathin g-C<sub>3</sub>N<sub>4</sub> nanosheets of ~600 μg/mL is extremely high, and the concentration used in practical bioimaging experimental testing is only ~150 μg/mL, which is much lower than this value.

Utilizing the good biocompatibility of the water-soluble ultrathin g-C<sub>3</sub>N<sub>4</sub> nanosheets, we carried out the bioimaging test by confocal fluorescence microscopy with excitation wavelength  $\lambda = 405$  nm, as shown in Figure 5b,c. The HeLa cells incubated with the ultrathin g-C<sub>3</sub>N<sub>4</sub> nanosheets do not weaken the cell activity and maintain their normal morphology. From Figure 5b,c, one can clearly see that the bright blue dots mainly adhere on the cell's membranes forming continuous circles as the morphology of the HeLa cells, indicating that the ultrathin g-C<sub>3</sub>N<sub>4</sub> nanosheets can be used as a promising biomarker for the labeling of the cell's membranes, which was further confirmed by the confocal fluorescence image of the HeLa cells labeled with ultrathin g-C<sub>3</sub>N<sub>4</sub> nanosheets and costained with 1,1'-dioctadecyl-3,3',3'-tetramethylindocarbocyanine perchlorate (DiI, 1 μg/mL) (Figure S13). Those results indicate that the as-exfoliated ultrathin g-C<sub>3</sub>N<sub>4</sub> nanosheets with good biocompatibility and nontoxicity can be used in bioimaging and further biomedical applications.

In summary, the ultrathin g-C<sub>3</sub>N<sub>4</sub> nanosheets have been successfully prepared by a "green" liquid exfoliation route from bulk g-C<sub>3</sub>N<sub>4</sub> in water for the first time. The ultrathin nanosheets show a size distribution ranging from 70 to 160 nm and a height of ~2.5 nm which is about seven C–N layers. Compared with bulk g-C<sub>3</sub>N<sub>4</sub>, the ultrathin nanosheets show enhanced photoabsorption and photoresponse, which not only enhance the intrinsic photocurrent and photocatalytic activity but also induce the extremely high PL quantum yield for ultrathin g-C<sub>3</sub>N<sub>4</sub> nanosheets up to 19.6%. Further study confirms that the water-soluble ultrathin g-C<sub>3</sub>N<sub>4</sub> nanosheets show excellent biocompatibility and nontoxicity. Benefiting from the inherent blue light PL with high quantum yields and high stability, good biocompatibility, and nontoxicity, the water-soluble ultrathin g-C<sub>3</sub>N<sub>4</sub> nanosheet is a brand-new but promising candidate for bioimaging application and may be further extended to biolabeling and biomedical applications.

## ■ ASSOCIATED CONTENT

### Supporting Information

Experimental details and characterization data. This material is available free of charge via the Internet at <http://pubs.acs.org>.

## ■ AUTHOR INFORMATION

### Corresponding Author

yxie@ustc.edu.cn

### Notes

The authors declare no competing financial interest.

## ■ ACKNOWLEDGMENTS

The authors thank the National Basic Research Program of China (2009CB939901), the Chinese Academy of Sciences (XDB01020300), and the National Natural Science Foundation of China (11079004 and 90922016) for financial support and Prof. Jun Wang and Dr. Hongxia Wang of the University of Science and Technology of China for bioimaging tests.

## ■ REFERENCES

- (1) (a) Novoselov, K. S.; Jiang, D.; Schedin, F.; Booth, T. J.; Khotkevich, V. V.; Morozov, S. V.; Geim, A. K. *Proc. Natl. Acad. Sci. U.S.A.* **2005**, *102*, 10451. (b) Geim, A. K.; Novoselov, K. S. *Nat. Mater.* **2007**, *6*, 183. (c) Loh, K. P.; Bao, Q.; Eda, G.; Chhowalla, M. *Nat. Chem.* **2010**, *2*, 1015. (d) Feng, J.; Peng, L.; Wu, C.; Sun, X.; Hu, S.; Lin, C.; Dai, J.; Yang, J.; Xie, Y. *Adv. Mater.* **2012**, *24*, 1917.
- (2) (a) Zhang, X.; Zhang, J.; Zhao, J.; Pan, B.; Kong, M.; Chen, J.; Xie, Y. *J. Am. Chem. Soc.* **2012**, *134*, 11908. (b) Schliehe, C.; Juarez, B. H.; Pelletier, M.; Jander, S.; Greshnykh, D.; Nagel, M.; Meyer, A.; Foerster, S.; Kornowski, A.; Klinke, C.; Weller, H. *Science* **2010**, *329*, 550. (c) Ramakrishna Matte, H. S. S.; Gomathi, A.; Manna, A. K.; Late, D. J.; Datta, R.; Pati, S. K.; Rao, C. N. R. *Angew. Chem., Int. Ed.* **2010**, *49*, 4059. (d) Ma, R.; Sasaki, T. *Adv. Mater.* **2010**, *22*, 5082.
- (3) (a) Wang, X.; Zhi, L.; Mullen, K. *Nano Lett.* **2007**, *8*, 323. (b) Feng, J.; Sun, X.; Wu, C.; Peng, L.; Lin, C.; Hu, S.; Yang, J.; Xie, Y. *J. Am. Chem. Soc.* **2011**, *133*, 17832. (c) Liu, Z.; Robinson, J. T.; Sun, X.; Dai, H. *J. Am. Chem. Soc.* **2008**, *130*, 10876. (d) Sreejith, S.; Ma, X.; Zhao, Y. *J. Am. Chem. Soc.* **2012**, *134*, 17346. (e) Yang, X.; Zhang, X.; Liu, Z.; Ma, Y.; Huang, Y.; Chen, Y. *J. Phys. Chem. C* **2008**, *112*, 17554.
- (4) (a) Zhang, Y.; Li, Y.; Yan, X.-P. *Small* **2009**, *5*, 185. (b) Gu, Y.-P.; Cui, R.; Zhang, Z.-L.; Xie, Z.-X.; Pang, D.-W. *J. Am. Chem. Soc.* **2011**, *134*, 79. (c) Zimmer, J. P.; Kim, S.-W.; Ohnishi, S.; Tanaka, E.; Frangioni, J. V.; Bawendi, M. G. *J. Am. Chem. Soc.* **2006**, *128*, 2526.
- (5) Soo Choi, H.; Liu, W.; Misra, P.; Tanaka, E.; Zimmer, J. P.; Itty Ipe, B.; Bawendi, M. G.; Frangioni, J. V. *Nat. Biotechnol.* **2007**, *25*, 1165.
- (6) (a) Liu, R.; Wu, D.; Feng, X.; Müllen, K. *J. Am. Chem. Soc.* **2011**, *133*, 15221. (b) Zhu, S.; Zhang, J.; Qiao, C.; Tang, S.; Li, Y.; Yuan, W.; Li, B.; Tian, L.; Liu, F.; Hu, R.; Gao, H.; Wei, H.; Zhang, H.; Sun, H.; Yang, B. *Chem. Commun.* **2011**, *47*, 6858.
- (7) Montigaud, H.; Tanguy, B.; Demazeau, G.; Alves, I.; Birot, M.; Dunogues, J. *Diam. Relat. Mater.* **1999**, *8*, 1707.
- (8) Groenewolt, M.; Antonietti, M. *Adv. Mater.* **2005**, *17*, 1789.
- (9) (a) Wang, X.; Maeda, K.; Thomas, A.; Takanebe, K.; Xin, G.; Carlsson, J. M.; Domen, K.; Antonietti, M. *Nat. Mater.* **2009**, *8*, 76. (b) Zhang, Y.; Antonietti, M. *Chem.—Asian J.* **2010**, *5*, 1307. (c) Su, F.; Mathew, S. C.; Lipner, G.; Fu, X.; Antonietti, M.; Blechert, S.; Wang, X. *J. Am. Chem. Soc.* **2010**, *132*, 16299. (d) Du, A.; Sanvito, S.; Smith, S. C. *Phys. Rev. Lett.* **2012**, *108*, 197207. (e) Du, A.; Sanvito, S.; Li, Z.; Wang, D.; Jiao, Y.; Liao, T.; Sun, Q.; Ng, Y. H.; Zhu, Z.; Amal, R.; Smith, S. C. *J. Am. Chem. Soc.* **2012**, *134*, 4393.
- (10) Sun, Y.; Cheng, H.; Gao, S.; Sun, Z.; Liu, Q.; Liu, Q.; Lei, F.; Yao, T.; He, J.; Wei, S.; Xie, Y. *Angew. Chem., Int. Ed.* **2012**, *57*, 8727.
- (11) Xu, T. G.; Zhang, C.; Shao, X.; Wu, K.; Zhu, Y. F. *Adv. Funct. Mater.* **2006**, *16*, 1599.
- (12) Madl, M.; Brezna, W.; Klang, P.; Andrews, A. M.; Strasser, G.; Smoliner, J. *Semicond. Sci. Technol.* **2010**, *25*, 065010.
- (13) (a) Coleman, J. N.; Lotya, M.; O'Neill, A.; Bergin, S. D.; King, P. J.; Khan, U.; Young, K.; Gaucher, A.; De, S.; Smith, R. J.; Shvets, I. V.; Arora, S. K.; Stanton, G.; Kim, H.-Y.; Lee, K.; Kim, G. T.; Duesberg, G. S.; Hallam, T.; Boland, J. J.; Wang, J. J.; Donegan, J. F.; Grunlan, J. C.; Moriarty, G.; Shmeliov, A.; Nicholls, R. J.; Perkins, J. M.; Grievson, E. M.; Theuwissen, K.; McComb, D. W.; Nellist, P. D.; Nicolosi, V. *Science* **2011**, *331*, 568. (b) Hernandez, Y.; Nicolosi, V.; Lotya, M.; Blighe, F. M.; Sun, Z.; De, S.; McGovern, I. T.; Holland, B.; Byrne, M.; un'Ko, Y. K.; Boland, J. J.; Niraj, P.; Duesberg, G.; Krishnamurthy, S.; Goodhue, R.; Hutchison, J.; Scardaci, V.; Ferrari, A. C.; Coleman, J. N. *Nat. Nanotechnol.* **2008**, *3*, 563.
- (14) Grimme, S. *J. Comput. Chem.* **2006**, *27*, 1787.
- (15) Lotsch, B. V.; Döblinger, M.; Sehnert, J.; Seyfarth, L.; Senker, J.; Oeckler, O.; Schnick, W. *Chem.—Eur. J.* **2007**, *13*, 4969.
- (16) Sun, Y.; Qu, B.; Liu, Q.; Gao, S.; Yan, Z.; Yan, W.; Pan, B.; Wei, S.; Xie, Y. *Nanoscale* **2012**, *4*, 3761.
- (17) Pan, D.; Zhang, J.; Li, Z.; Wu, M. *Adv. Mater.* **2010**, *22*, 734.